HIGH SCHOOL EDITION
Journal of Student Research
Volume 11 Issue 4 (2022)

# Metal Ion Sensing by BAPTA: Investigation Using $^1$H Nuclear Magnetic Resonance Spectroscopy

Sunayna Adoni[1], Trivikram R. Molugu[#], and Tatyana I. Igumenova[#]

[1]The Liberal Arts and Science Academy, Austin, Texas, USA
[#]Advisor

## ABSTRACT

Many biological macromolecules rely on metal ions to maintain structural integrity and control their regulatory function. In biological fluids, detection and identification of metal ions requires sensitive analytical tools with clear readouts. In this work, we sought to investigate the potential of solution Nuclear Magnetic Resonance (NMR) spectroscopy to analyze metal ion solutions and mixtures. To enable $^1$H NMR detection, we prepared the complexes of eight metal ions with the chelating agent, 1,2-bis(o-aminophenoxy)ethane-N,N,N′,N′-tetraacetic acid (BAPTA). The $^1$H NMR spectra were collected for BAPTA samples as a function of metal ion concentrations. The analysis of NMR data revealed that all metal ions with a notable exception of $Mg^{2+}$ bind BAPTA with high affinities and form complexes with 1:1 metal-to-chelator stoichiometry. Both methylene and aromatic regions of the BAPTA $^1$H NMR spectra experience significant changes upon the metal ion complex formation. We identified the spectroscopic signatures of trivalent and paramagnetic ions and demonstrated that the binary $Zn^{2+}$/$Pb^{2+}$ metal ion mixture can be successfully analyzed by NMR. We conclude that complexation with BAPTA followed by the $^1$H NMR analysis is a sensitive method to detect and identify both nutritive and xenobiotic metal ions.

## Introduction

Metal ions play an important role in biological systems. They can function as catalysts, structural cofactors, and signaling molecules. Metal ion deficiencies are associated with numerous human pathologies (Moustakas, 2021). Some heavy metal ions are considered environmental toxins, and enter the environment through the soil erosion, mining, and sewage discharge (Jaishankar et al., 2014).

In general, metal ions can be divided into two groups: nutritive and xenobiotic. Nutritive metal ions are involved in maintenance and regulation of important biochemical processes, such as electron transfer reactions (Parrish & Wang, 2010), neurotransmitter release, and enzymatic catalysis. The examples of nutritive metal ions include calcium, magnesium, iron, copper, zinc, manganese, and cobalt. However, they are only beneficial in the needed amounts. Excess of nutritive metal ions can cause harmful conditions. For example, excess calcium causes hypercalcemia, negatively affecting the bones, nervous system, and digestive system (Mayo Clinic, 2022).

Metal ions that have no nutritive value are defined as xenobiotic. Some examples are lead, cadmium, manganese, thallium, mercury, and radioactive metals. Exposure to xenobiotic metal ions is extremely harmful, and can result in nervous system disorders, organ failure, and some cancers ((Landrigan & Todd, 1994) and (Genchi et al., 2020)).

Xenobiotic metal ions are potent environmental toxins because they can bind to the biological macromolecules in lieu of nutritive metal ions. By engaging in such ionic mimicry, xenobiotic ions interfere with vital protein functions.

The toxicity of xenobiotic metal ions is most aptly illustrated by lead (Pb). Pb is used in many agricultural and industrial processes, creating opportunities for harmful exposure. Although the use of lead in paints and ceramics has decreased significantly over the years, about 25% of U.S. homes still have significant lead-based hazards in the form of dust or deteriorating paint (Jacobs et al., 2002). Pb is toxic to most organ systems and is known to cause delayed development of the nervous system and diminished intelligence ((Landrigan & Todd, 1994) and (Garza-Lombo et al., 2018)).

Chelators are defined as molecules with high affinities for metal ions. Chelators have found widespread clinical applications (Kontoghiorghes, 2020) due to their high efficiency in metal detoxification (Blanusa et al., 2005). Chelators have been applied to alleviate the toxic effects of xenobiotic metal exposure from contamination in food and drink products, dust, and pollution. The use of chelators also allows to effectively treat health conditions associated with excessive amounts of nutritive ions such as calcium. Traditional metal chelators include EDTA, EGTA, and 2,3-dimercaprol (Flora & Pachauri, 2010). Some chelators show high specificity towards certain metal ions. For example, 1,2-bis(o-aminophenoxy) ethane-N,N,N′,N′-tetraacetic acid (BAPTA) is a chelator with high specificity to $Ca^{2+}$ ions (Tsien, 1980).

BAPTA is a cell-impermeable chelator that is used to regulate calcium levels by removing bound metal ions from macromolecules. It shows high selectivity to calcium over magnesium (Zhou et al., 2021), and its metal ion-binding properties are less sensitive to pH than those of the other chelators. Treatment of cells with membrane permeable BAPTA derivative was found to protect them from calcium overload (Collatz et al., 1997). The metal ion-binding properties of the BAPTA-like chelators have been studied using various biophysical methods (Britigan et al. 1998, Grynkiewiez et al. 1985, Csomos et al. 2021, Zhou et al. 2021), such as UV-vis absorption, electron spin resonance, and fluorescence spectroscopies. Nuclear Magnetic Resonance (NMR) spectroscopy has been extensively applied to investigate intracellular free metal ions, using the fluorinated analogs of BAPTA (Schanne et al. 1990, Kuchel et al. 2021, Bar-Shir et al. 2013). However, the investigations of BAPTA and its interactions with metal ions have been limited (Tsien, 1980). Here, we fill this void by identifying the spectroscopic signatures of BAPTA-metal ion interactions.

### Question Addressed and Hypothesis

The objective of the present work was to establish the spectroscopic signatures of metal ion binding to the BAPTA chelating agent and evaluate the use of NMR spectroscopy as an analytical tool to characterize metal ion mixtures. NMR spectroscopy was chosen because of its: (i) non-invasive nature, (ii) sensitivity of $^{1}H$ chemical shifts to the changes of electronic environment caused by the binding events, and (iii) potential applicability to the biological samples and fluids. Our hypothesis is that the $^{1}H$ resonances of BAPTA are sensitive to the chemical identity of the metal ion and report on the affinities and stoichiometries of the interactions. To test this hypothesis, we chose both nutritive: $Ca^{2+}$, $Zn^{2+}$, $Mn^{2+}$, $Ni^{2+}$, and $Mg^{2+}$; and xenobiotic: $Cd^{2+}$, $Pb^{2+}$, and $La^{3+}$ metal ions. Among the selected set, $Mn^{2+}$ and $Ni^{2+}$ are paramagnetic (i.e. have an unpaired electron), and $La^{3+}$ is trivalent.

## Materials and Methods

## Materials

All reagents were obtained from Sigma Aldrich (St. Louis, MO). Deionized Milli-Q water was treated with Chelex-100 resin to remove trace metal ions. The following salts were used to make the metal ions solutions: $ZnCl_2$ (zinc chloride), $CaCl_2$ (calcium chloride), $LaCl_3 \cdot 7H_2O$ (lanthanum chloride heptahydrate), $MnCl_2$ (manganese chloride), $Pb(NO_3)_2$ (lead nitrate), $Cd(NO_3)_2$ (cadmium nitrate), $NiSO_4 \cdot 6H_2O$ (nickel sulfate hexahydrate), and $MgCl_2$ (magnesium chloride). BAPTA was acquired in the acid form and dissolved in DMSO-$d_6$ to make a stock solution.

## Preparation of reagent solutions

All metal ion solutions were prepared in 10 mL volumetric flasks using decalcified Milli-Q water comprising 90% $H_2O$ and 10% $D_2O$ at pH 7.0. $D_2O$ was added to provide a lock signal for the NMR spectrometer. The quantities of the metal ion salts required for the preparation of 10 mM stock solutions are given in **Table 1**. All metal ion salts could be fully dissolved in water at pH 7.0 except for $ZnCl_2$ and $Cd(NO_3)_2$. Trace amounts of HCl were added to these solutions to achieve full solubilization. Final pH values of the stock solutions ranged from 6.2 to 7.3 (**Table 1**). 40 mM BAPTA stock solution was prepared by dissolving 9.5 mg of BAPTA acid in 0.5 mL of DMSO-$d_6$. The stock solutions of metal ions and BAPTA were used to generate the appropriate dilutions for the NMR samples.

## NMR Spectroscopy

NMR experiments were conducted on a Bruker Avance NEO instrument operating at the $^1$H Larmor frequency of 600 MHz. The temperature was calibrated using methanol-$d_4$ and set at 25 $^o$C. The $^1$H NMR spectra were recorded with 8192 points in the time domain and the spectral width of 16 ppm. For each spectrum, we collected 64 scans with a recycle delay of 10 s. $^1$H water signal at 4.69 ppm was suppressed with the excitation sculpting pulse sequence (Hwang & Shaka, 1995). The data were zero-filled to 32,768 points, apodized with a 3 Hz Gaussian function, and Fourier transformed. All data processing and peak integration were conducted using the MestReNova software package (Willcott, 2009). The simulation of the $^1$H BAPTA spectrum was carried out using "NMR Predict" online tool (www.nmrdb.org) (Binev et al. 2007).

The concentration of BAPTA in metal ion titration experiments was 0.1 mM in all cases. The NMR sample of free BAPTA was prepared by 100-fold dilution of the 10 mM DMSO-$d_6$ stock solution with water. NMR-monitored titration experiments were carried out by adding small aliquots of metal ion solutions to the BAPTA sample. The dilution of the BAPTA NMR sample did not exceed 10% at the end of the titrations. The fraction of metal ion-bound BAPTA, f, was calculated as: $f=1-(A/A_0)$, where A and $A_0$ are the areas under the methylene $^1$H peak in the metal-containing and metal-free BAPTA solutions, respectively. The fraction of free BAPTA was calculated as the $A/A_0$ ratio. The error bars in **Fig. 2** were estimated using the standard deviation of the area under the residual $^1$H peak of DMSO-$d_6$ at 2.6 ppm.

**Table 1.** Preparation of metal ion stock solutions.

| Metal ion salt | Amount of salt per 10 mL (mg) | pH |
|---|---|---|
| $CaCl_2$ | 11.0 | 6.9 |
| $ZnCl_2$ | 68.1 | 6.9 |
| $Pb(NO_3)_2$ | 33.1 | 6.2 |

| | | |
|---|---|---|
| $Cd(NO_3)_2$ | 30.8 | 6.6 |
| $NiSO_4 \cdot 6H_2O$ | 26.3 | 7.3 |
| $MnCl_2$ | 39.6 | 6.3 |
| $LaCl_3 \cdot 7H_2O$ | 37.1 | 6.6 |
| $MgCl_2$ | 20.3 | 6.9 |

## Results

### Resonance assignments of the BAPTA $^1$H NMR spectrum

The BAPTA molecules contains both aromatic and methylene $^1$H atoms. The first step was to associate the $^1$H signals of BAPTA with specific chemical groups in a process called resonance assignment. As expected, the $^1$H spectrum of BAPTA contains several peaks (blue trace of **Fig. 1**). The peak at 2.6 ppm corresponds to the residual $^1$H of DMSO-$d_6$, as is evident from the comparison with the DMSO-$d_6$-only spectrum (red trace of **Fig. 1**). To facilitate the assignment of the remaining BAPTA peaks, we simulated its spectrum and compared it with the experimental data. The signal of aromatic protons falls in the range between 6.9 and 7.1 ppm. The methylenes adjacent to the metal-coordinating carboxyl groups are predicted to resonate at 3.91 ppm, which matches well the experimentally observed value of 3.92 ppm. The $^1$H of methylene groups that bridge the aromatic rings are predicted to resonate at 4.2 ppm. In the experimental spectrum, we observe a very small peak at 4.37 ppm. The likely cause of such low intensity is the relaxation properties of this molecular site. The spectrum of free BAPTA was used as a reference to evaluate chemical shift perturbations due to metal ion binding.

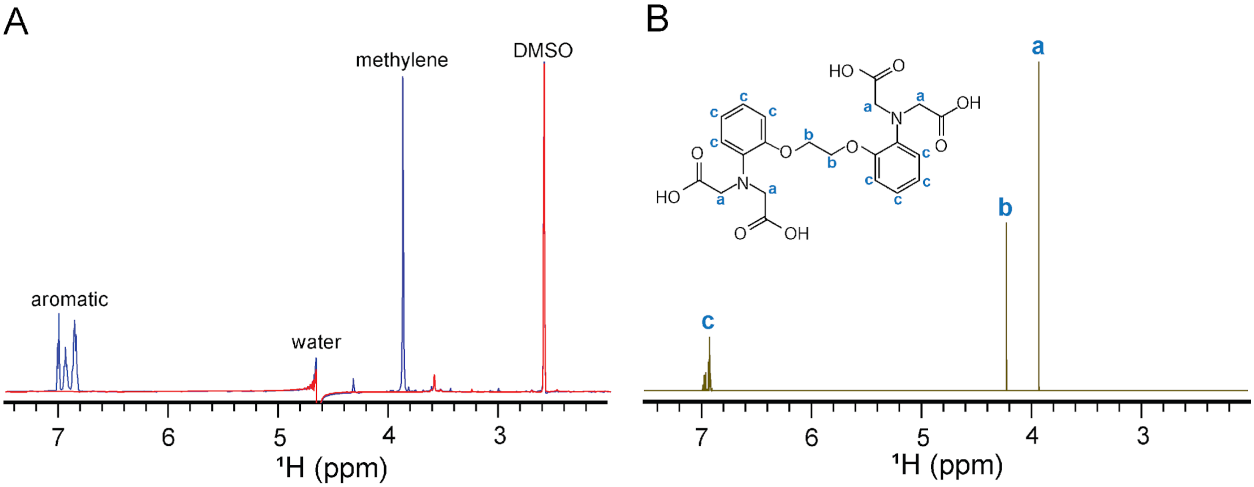


**Figure 1.** Chemical structure and $^1$H resonance assignments of BAPTA. **(A)** The $^1$H NMR spectra of 0.1 mM BAPTA and DMSO-$d_6$ (dissolved in decalcified water) are shown as blue and red traces, respectively. The chemical shift positions of aromatic and methylene $^1$H resonances are labeled. The suppressed water signal appears as a dispersive peak at 4.69 ppm. **(B)** A simulated $^1$H NMR spectrum is presented for comparison with the experimental data.

### $^1$H methylene BAPTA peaks are sensitive reporters of divalent metal ion binding

To characterize the spectroscopic response of BAPTA to $Ca^{2+}$ and $Mg^{2+}$ binding, the metal ions were added stepwise to the sample of free BAPTA to generate the BAPTA:$M^{2+}$ ratios up to 8-fold molar excess. For both metal ions, significant changes were observed in all regions of the NMR spectra, yet the response to $Ca^{2+}$ and $Mg^{2+}$ was drastically different. The spectroscopic responses are illustrated using the region of the NMR spectrum that contains the methylene signal of BAPTA (**Fig. 2A,B**). Addition of $Ca^{2+}$ resulted in the decrease of the $^1$H methylene peak intensity (**Fig. 2A**). The data were quantified as described in Materials and Methods to obtain the $Ca^{2+}$-binding curve of **Fig. 2C** (black squares). The $Ca^{2+}$ binding curve shows saturable behavior at stoichiometric (i.e. 1:1) ratio of BAPTA to $Ca^{2+}$, indicating tight binding regime. In contrast, we were not able to saturate BAPTA with $Mg^{2+}$ even at 8-fold molar excess. The kinetics of $Mg^{2+}$ binding to BAPTA falls into the intermediate exchange regime, making peak integration at high $Mg^{2+}$ excess difficult. However, the data analysis of up to 0.4 mM concentration of $Mg^{2+}$ enabled us to generate a binding curve shown in **Fig. 2C** (purple circles). Fractional saturation of only ~20% was achievable at 4-fold molar excess of $Mg^{2+}$ relative to BAPTA, indicating very low affinity of $Mg^{2+}$-BAPTA interactions.

Using the same experimental approach as described above for $Mg^{2+}$ and $Ca^{2+}$, we collected and analyzed the data for other metal ions: $Zn^{2+}$, $Mn^{2+}$, $Pb^{2+}$, $Cd^{2+}$, and $Ni^{2+}$. The results of the analysis are collectively presented in **Fig. 2D**, using the fractional population of metal ion-free BAPTA as a readout. The data clearly illustrate that all divalent metal ions tested in this work, with a notable exception of $Mg^{2+}$, have extremely high affinity to BAPTA, resulting in almost full saturation at stoichiometric ratios. In aggregate, our results attest to the exquisite sensitivity of $^1$H NMR to the BAPTA interactions with metal ions.

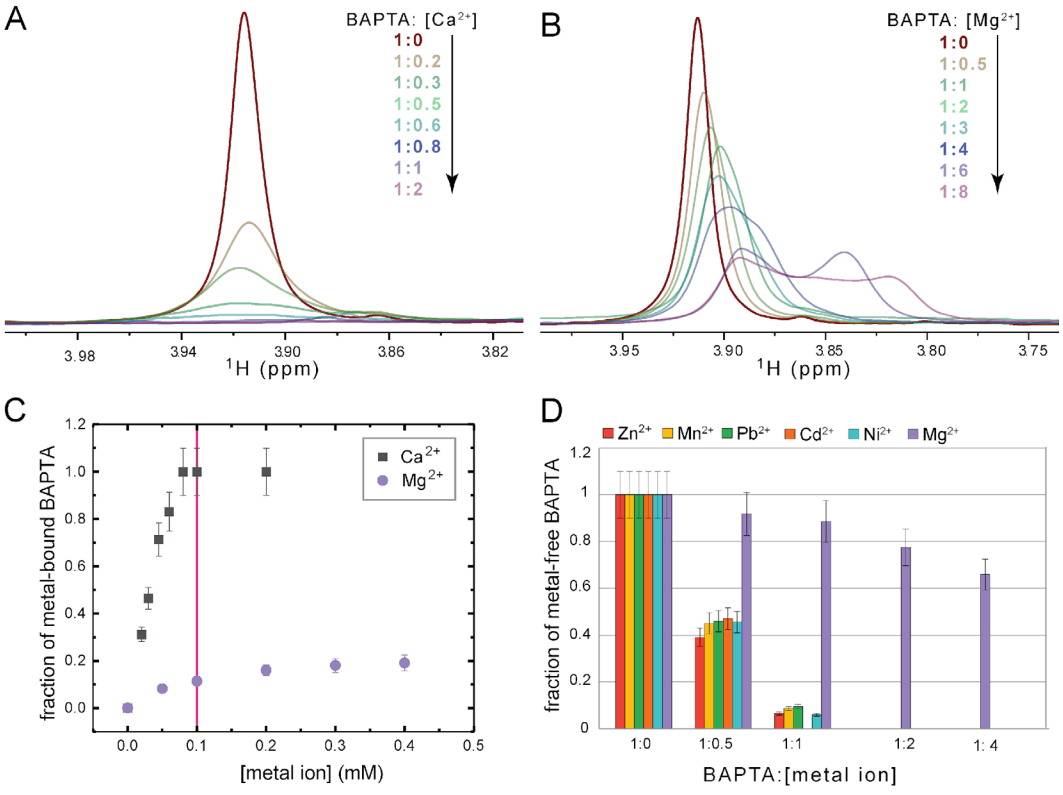


**Figure 2.** Detection of BAPTA-metal ion interactions by $^1$H NMR. The response of the BAPTA $^1$H methylene peak to increasing concentration of metal ions is shown for $Ca^{2+}$ **(A)** and $Mg^{2+}$ **(B)**. The molar ratios of BAPTA to metal

ion are color-coded. **(C)** The fractional population of metal ion-bound BAPTA plotted against the total concentration of metal ions. Full saturation of the chelator by $Ca^{2+}$ is attained at equimolar concentrations, while only ~20% of the chelator is bound at 4-fold molar excess of $Mg^{2+}$. Red line marks the equimolar concentration point. **(D)** Fractional populations of free BAPTA obtained in NMR-detected binding experiments with $Zn^{2+}$, $Mn^{2+}$, $Pb^{2+}$, $Cd^{2+}$, $Ni^{2+}$, and $Mg^{2+}$. Of all metal ions tested, $Mg^{2+}$ has the lowest affinity to BAPTA.

## $^1$H NMR signatures produced by paramagnetic and trivalent metal ion binding to BAPTA

Two metal ions of the chosen set are paramagnetic: $Mn^{2+}$ and $Ni^{2+}$. Paramagnetic metal ions contain at least one unpaired electron. If an unpaired electron is near the nucleus being detected by NMR, the electron-nuclear interactions will cause a rapid decay of nuclear magnetization. This in turn will result in significant broadening of the $^1$H peaks in the NMR spectra. To evaluate the effect of paramagnetic ions on the spectrum of BAPTA, we collected the data for several BAPTA:metal ion ratios (**Fig. 3**). The BAPTA response to binding $Mn^{2+}$ and $Ni^{2+}$ is illustrated using the aromatic region of the spectrum that is centered around 7 ppm. For both metal ions, we observed uniform broadening of aromatic $^1$H peaks as the metal ion concentration increases (**Fig. 3**). The signal almost completely disappeared at equimolar concentrations of BAPTA and $Mn^{2+}$ or $Ni^{2+}$. We conclude that BAPTA is a sensitive probe for the detection of paramagnetic metal ions, where the readout is the broadening and subsequent disappearance of NMR peaks due to the proximity to the unpaired electron.

One of the metal ions of the chosen set, $La^{3+}$, is trivalent. To determine if $La^{3+}$ binding produces distinct signatures in the $^1$H NMR spectrum, we recorded the spectra at several chelator-to-metal ion ratios. The BAPTA response to the interactions with $La^{3+}$ is striking (**Fig. 4**). Most of the aromatic protons experience a downfield shift, especially evident for the group of peaks that appears between 7.2 and 7.3 ppm. Of note, at sub-stoichiometric concentrations of $La^{3+}$, we detect the $^1$H signals of both, free and $La^{3+}$-complexed BAPTA. This observation reports that the aromatic protons of free and $La^{3+}$-complexed BAPTA are in slow exchange on the NMR chemical shift timescale.

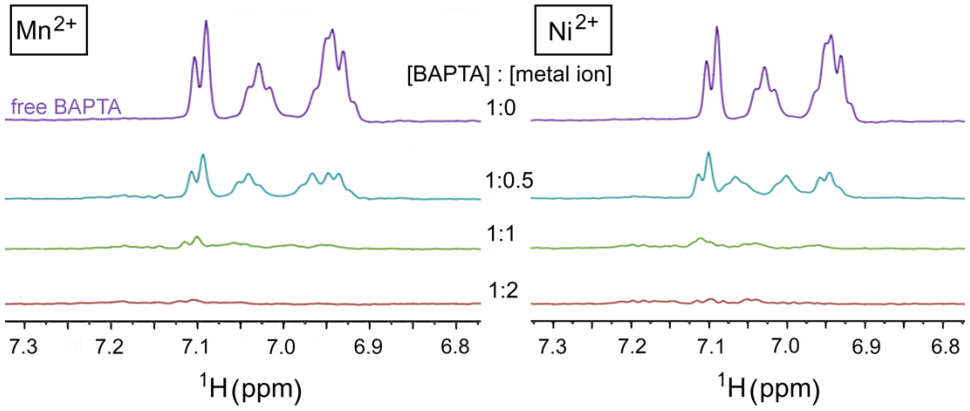


**Figure 3.** Aromatic regions of the $^1$H NMR spectra of $Mn^{2+}$- and $Ni^{2+}$-complexed BAPTA. The spectra of metal-free BAPTA are shown in purple for reference. Upon progressive increase of metal ion concentration, the intensity of the $^1$H resonances decreases due to the paramagnetic relaxation enhancement caused by the presence of unpaired electrons in $Mn^{2+}$ (left panel) and $Ni^{2+}$ (right panel).

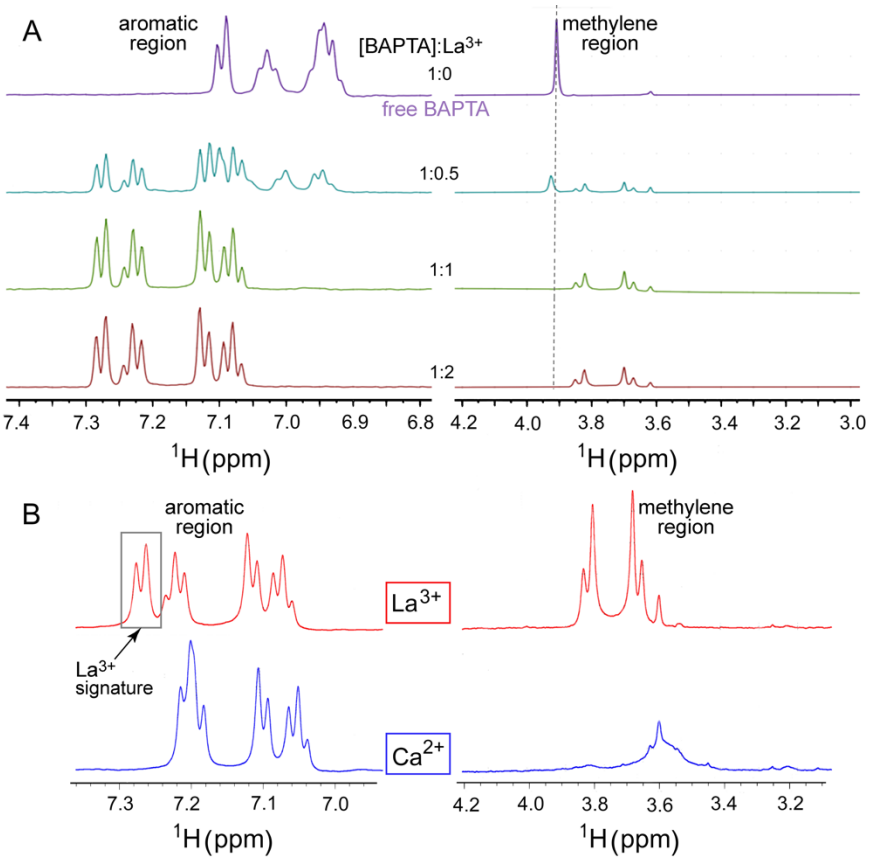


**Figure 4.** $^{1}$H NMR signatures of the $La^{3+}$-BAPTA complex. **(A)** Changes in the $^{1}$H NMR spectra of BAPTA upon increasing $La^{3+}$ concentration. Both, aromatic (left panel) and methylene (right panel) regions show drastic changes. The stoichiometry of complex formation is 1:1. **(B)** Comparison of the $^{1}$H NMR spectra of $La^{3+}$-BAPTA (red) and $Ca^{2+}$-BAPTA (blue) complexes. The molar ratio of metal ion to chelator is 1:1. Both aromatic and methylene regions contain spectroscopic signatures that can be used to identify the $La^{3+}$-bound species.

In addition to the drastic changes in the aromatic region of the spectrum, the methylene protons are significantly affected by $La^{3+}$ binding. The $^{1}$H methylene peak of $La^{3+}$-complexed BAPTA is split into four distinct peaks that are shifted upfield (right panels of **Fig. 4A,B**). The chemical equivalency of the $^{1}$H BAPTA resonances is therefore broken by the interactions with $La^{3+}$. The stoichiometry of the $La^{3+}$-BAPTA complex is 1:1, and the interactions are high-affinity, based on the identity of the NMR spectra collected at 1:1 and 1:2 BAPTA-to-$La^{3+}$ ratios.

Comparison of the $Ca^{2+}$- and $La^{3+}$-complexed BAPTA spectra emphasizes the differences in both aromatic and methylene regions (**Fig. 4B**), suggesting that $^{1}$H NMR of BAPTA complexes is a useful analytical tool to identify spectroscopic signatures of different metal ions. To validate this conclusion, we investigated the binary mixtures of $Pb^{2+}$ and $Zn^{2+}$, as described in the next section.

## $^{1}$H NMR characterization of the $Pb^{2+}$/$Zn^{2+}$ metal ion mixture

The power of NMR as an analytical tool lies in its ability to produce distinct spectroscopic signatures of analytes. We sought to evaluate the binary mixture of $Pb^{2+}$ and $Zn^{2+}$ to determine if these metal ions are identifiable by $^{1}$H NMR

of their BAPTA complexes. $Pb^{2+}$ was selected because it is a potent environmental toxin whose reliable detection in biological fluids is essential. $Pb^{2+}$ can bind to macromolecules in lieu of $Zn^{2+}$ and $Ca^{2+}$, and thereby interfere with macromolecular function. The sample chosen for this study represents a mixture of a nutritive metal ion, $Zn^{2+}$, and its xenobiotic competitor, $Pb^{2+}$.

The $^1H$ NMR spectrum of 0.1 mM BAPTA and $Pb^{2+}/Zn^{2+}$ mixture (purple) is contrasted with those of $Pb^{2+}$-BAPTA (teal) and $Zn^{2+}$-BAPTA (red) complexes in **Fig. 5**. The data clearly show that the spectrum of BAPTA/$Pb^{2+}/Zn^{2+}$ mixture is close to the sum of $Pb^{2+}$-BAPTA and $Zn^{2+}$-BAPTA spectra, suggesting that $Pb^{2+}$ and $Zn^{2+}$ have similar affinities to BAPTA. Moreover, the $^1H$ resonances that are specific to a given metal ion can be identified: the peaks at 7.08, 7.18, and 7.20 ppm are unique to the $Pb^{2+}$-BAPTA complex, and the group of peaks centered at 6.97 ppm is unique to the $Zn^{2+}$-BAPTA complex. We conclude that $^1H$ NMR spectroscopy is a useful analytical method to identify the nutritive and xenobiotic metal ions in solution.

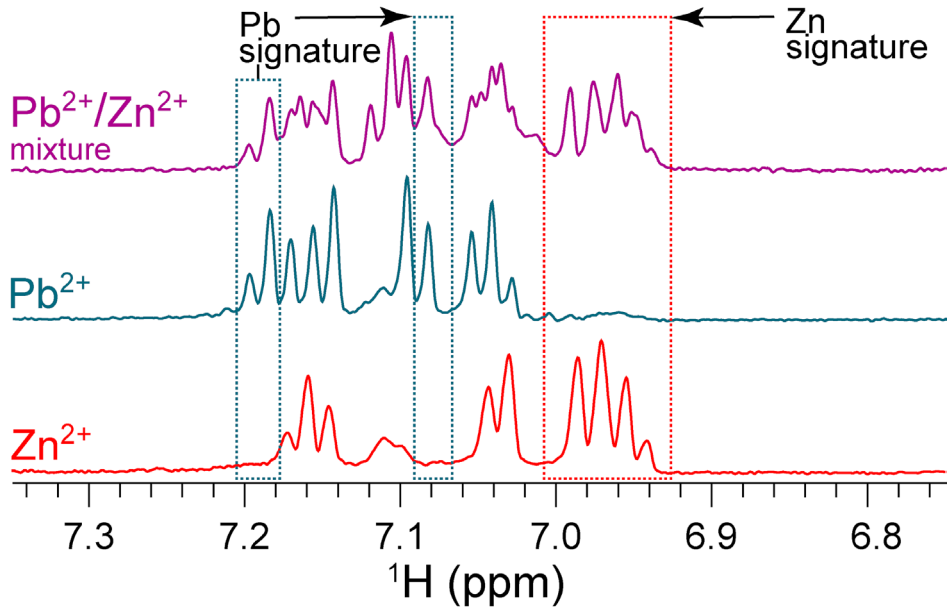


**Figure 5.** $^1H$ NMR of the $Pb^{2+}/Zn^{2+}$ mixture identifies metal ion-specific spectroscopic signatures. Shown are the aromatic regions of the $^1H$ NMR spectra of 0.1 mM BAPTA/0.05 mM $Pb^{2+}$/0.05 mM $Zn^{2+}$ ($Pb^{2+}/Zn^{2+}$ mixture, purple), 0.1 mM BAPTA/0.1 mM $Pb^{2+}$ (teal), and 0.1 mM BAPTA/0.1 mM $Zn^{2+}$. The $^1H$ resonances that are specific to $Pb^{2+}$-BAPTA and $Zn^{2+}$-BAPTA are highlighted with teal and red rectangles, respectively.

## Discussion

In this work, we sought to investigate the potential of solution NMR spectroscopy to analyze metal ion solutions and mixtures, using BAPTA as a chelating agent. The formation of high-affinity complexes with BAPTA is a prerequisite for the success of such analysis. All nutritive metal ions but $Mg^{2+}$ showed high affinity interactions with BAPTA (**Fig. 2D**). The behavior of $Mg^{2+}$ is contrasted with that of $Ca^{2+}$ (**Figs. 2A-C**), that forms a tight BAPTA complex with a coordination number of 8 (Bootman et al., 2018). Our data on relative $Ca^{2+}/Mg^{2+}$ affinities are consistent with the reported dissociation constants of $10^{-7}$ M for $Ca^{2+}$ and $10^{-2}$ M for $Mg^{2+}$ (Tsien, 1980). The $Ca^{2+}/Mg^{2+}$ selectivity of BAPTA is intriguing because $Mg^{2+}$ has a smaller size and higher charge density than $Ca^{2+}$. $Mg^{2+}$ is therefore expected to bind more tightly to the carboxylate groups present in BAPTA. Such a discrepancy in metal ion specificity was previously explained by many-body polarization effects (Jing et al. 2018). For the analysis of both strong and weak binding, the uncrowded methylene region of the $^1H$ NMR spectrum is particularly advantageous. However, the aromatic region, despite its complexity, is also information rich. This is illustrated by the drastic spectral changes that take place during the titration of BAPTA with $Ca^{2+}$ (**Fig. 6**). Of note, at sub-stoichiometric concentrations of $Ca^{2+}$ several aromatic protons enter the intermediate exchange regime on the NMR chemical shift timescale. The intermediate exchange regime is characterized by the broadening of the NMR peaks and occurs when the difference in chemical shifts is comparable to the sum of the forward and reverse kinetic rate constants for the interconversion reaction between free and $Ca^{2+}$-bound BAPTA.

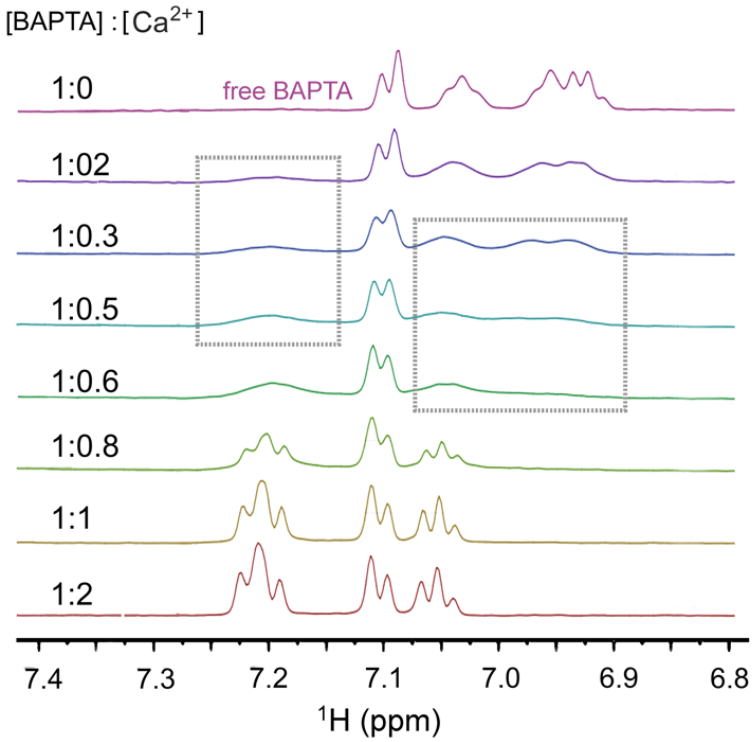


**Figure 6.** Illustration of the intermediate exchange behavior for the interconversion between free and $Ca^{2+}$-complexed BAPTA. The intermediate exchange regime is observed between 2 and 60% $Ca^{2+}$ saturation of BAPTA and manifests itself as significant peak broadening (highlighted with rectangles) in the aromatic region of the spectrum.

The paramagnetic nutritive metal ions, $Mn^{2+}$ and $Ni^{2+}$ elicited a drastic response in the $^{1}H$ BAPTA spectrum by broadening the $^{1}H$ resonances of the aromatic BAPTA region. The observed line broadening is useful for the general detection of paramagnetic metal ions, but not for establishing their identities: $Mn^{2+}$ and $Ni^{2+}$ BAPTA complexes show very similar spectroscopic signatures.

Among the xenobiotic metal ions, we highlight our results on $La^{3+}$ and $Pb^{2+}$. Both metal ions form 1:1 complexes with BAPTA because there are no detectable spectral changes when the metal ion is added in molar excess relative to the chelating agent. Compared to $Ca^{2+}$, $La^{3+}$-BAPTA complex shows distinct $^{1}H$ chemical shift patterns for both aromatic and methylene regions (**Fig. 4B**). The latter is especially notable, as the interactions of $La^{3+}$ with BAPTA relieve the chemical equivalency of the methylene protons, leading to the idea that this could be a useful NMR signature of trivalent metal ions. With respect to $Pb^{2+}$, we evaluated the ability of NMR to identify the presence of $Pb^{2+}$ in a binary mixture with a nutritive metal ion, $Zn^{2+}$. $Pb^{2+}$ is a potent environmental toxin that competes with $Zn^{2+}$ and $Ca^{2+}$ for sulfur- and oxygen-rich metal ion coordination sites in biomacromolecules. The characterization of the $Pb^{2+}/Zn^{2+}$ mixture (**Fig. 5**) revealed that there are $^{1}H$ peaks/groups of peaks that are specific to the metal ion type, attesting to the applicability of NMR to the analysis of the binary divalent metal ion mixtures. NMR analysis of more complex mixtures will require a full set of reference spectra for individual metal ions and application of spectral deconvolution procedures.

In summary, through the systematic analysis of the $^{1}H$ NMR spectra of the metal ion-BAPTA complexes we demonstrated how this method can be applied to the analysis of metal ions solutions and mixtures. Most metal ions tested (that belong to nutritive and xenobiotic groups) bind BAPTA with high affinity and produce unique spectroscopic signatures.

## Conclusions

The main conclusion of this work is that the use of chelating agent BAPTA in combination with $^{1}H$ NMR is a sensitive analytical tool to detect and identify metal ions in solution. We demonstrated the applicability of this approach using a set of metal ions that have different biological roles and chemical properties. Out of 8 metal ions tested, only $Mg^{2+}$ has too low of an affinity to be readily detectable through BAPTA complexation. Both methylene and aromatic regions of the $^{1}H$ NMR spectra of BAPTA complexes can be used for detection and identification of metal ions in solution. One of the promising future directions is to investigate the NMR properties of cell-permeable chelators complexed to metal ions. Of particular interest are fluorinated chelators, due to high sensitivity of the $^{19}F$ nucleus and background-free NMR detection when used in the analysis of biological fluids.

## Acknowledgments

This work was supported by the NSF grant CHE-1905116 to T.I.I. S.A. thanks Dr. Sachin Katti and Ms. Xiao-Ru Chen for helpful discussions and assistance with computer setup.

## References

Binev,Y. Marques, M.M., Aires-de-Sousa, J., Prediction of 1H NMR coupling constants with associative neural networks trained for chemical shifts J. Chem. Inf. Model. 2007, 47, 2089-2097. https://doi.org/10.1021/ci700172n

Blanusa, M., Varnai, V. M., Piasek, M., & Kostial, K. (2005). Chelators as antidotes of metal toxicity: therapeutic and experimental aspects. *Current Medicinal Chemistry*, *12*(23), 2771-2794. http://dx.doi.org/10.2174/092986705774462987

Bootman, M. D., Allman, S., Rietdorfa, K., Bultynck, G. (2018) *Cell Calcium* (73) 82–87. https://doi.org/10.1006/scdb.2000.0211

Britigan, B. E., Rasmussen, G. T., Cox, C. D. (1998). Binding of Iron and Inhibition of Iron-Dependent Oxidative Cell Injury by the "Calcium Chelator" 1,2-Bis(2-Aminophenoxy)Ethane N,N,N′,N′-tetraacetic Acid (BAPTA)**.** *Biochemical Pharmacology*, 55, 287–295. https://doi.org/10.1016/S0006-2952(97)00463-2

Collatz, M.B., Rudel, R., & Brinkmeier, H. (1997). Intracellular calcium chelator BAPTA protects cells against toxic calcium overload but also alters physiological calcium responses. *Cell Calcium*, *21*(6), 453-459. https://doi.org/10.1016/S0143-4160(97)90056-7

Flora, S. J.S., & Pachauri, V. (2010). Chelation in Metal Intoxication. *International Journal of Environmental Research and Public Health*, *7*(7), 2745-2788. https://doi.org/10.3390%2Fijerph7072745

Garza-Lombo, C., Posadas, Y., Quintanar, L., Gonsebatt, M. E., & Franco, R. (2018). Neurotoxicity Linked to Dysfunctional Metal Ion Homeostasis and Xenobiotic Metal Exposure: Redox Signaling and Oxidative Stress. *Antioxidants & Redox Signaling*, *28*(18), 1669-1703. https://doi.org/10.1089%2Fars.2017.7272

Genchi, G., Carocci, A., Lauria, G., Sinicropi, M. S., & Catalano, A. (2020). Nickel: Human Health and Environmental Toxicology. *International Journal of Environmental Research and Public Health*, *17*(3), A599-A606. https://doi.org/10.1289%2Fehp.021100599

Grynkiewicz, G., Poenie,M., Tsien ,R.Y., (1985) A new generation of Ca2+ indicators with greatly improved fluorescence properties *Journal of Biological Chemistry* 260(6):3440-50. https://doi.org/10.1016/S0021-9258(19)83641-4

Hwang, T.-L., Shaka, A.J. (1995) *Journal of Magnetic Resonance*, 112 275-279. https://doi.org/10.1006/jmra.1995.1047

Jacobs, D.E., Clickner, R.P., Zhou,J.Y., Viet, S.M. Marker, D.A., Rogers, J. W., Zeldin, D.C., Broene, P. & Friedman, W. (2002) *Environmental Health Perspectives* 110, A599 – A606. https://doi.org/10.1289%2Fehp.021100599

Jaishankar, M., Tseten, T., Anbalagan, N., Mathew, B. B., & Beeregowda, K. N. (2014). Toxicity, mechanism and health effects of some heavy metals. *Interdisciplinary Toxicology*, *7*(2), 60-72. https://doi.org/10.2478/intox-2014-0009

Jing, Z. C., Qi, L. R. and Ren, P (2018), Many-body effect determines the selectivity for $Ca^{2+}$and $Mg^{2+}$in proteins. *Proceedings of the National Academy of Sciences USA,* 115 E7495–E7501 https://doi.org/10.3390/ijerph17030679

Kontoghiorghes, G. J. (2020). Advances on Chelation and Chelator Metal Complexes in Medicine. *International Journal of Molecular Sciences*, *21*(7), 2499.https://doi.org/10.3390%2Fijms21072499

Landrigan, P. J., & Todd, A. C. (1994). Lead Poisoning. *The Western Journal of Medicine*, *161*(2), 153-159. https://pubmed.ncbi.nlm.nih.gov/7941534/

Mayo Clinic. (2022, March 23). *Hypercalcemia - Symptoms and causes*. Mayo Clinic. Retrieved August 2, 2022, from https://www.mayoclinic.org/diseases-conditions/hypercalcemia/symptoms-causes/syc-20355523

Moustakas, M. (2021). The Role of Metal Ions in Biology, Biochemistry and Medicine. *Materials*, *14*(3), 549. https://doi.org/10.3390/ma14030549

Parrish, A. R., & Wang, L. (2010). Genetic Incorporation of Unnatural Amino Acids into Proteins. *Comprehensive Natural Products II*, 5(1), 587-617. https://doi.org/10.1016/B978-008045382-8.00694-8

Schanne, F. a., Dowd, T. l., Gupta, R. K., & Rosen, J. f. (1990). Development of $^{19}F$ NMR for measurement of $[Ca^{2+}]_i$ and $[Pb^{2+}]_I$ in cultured osteoblastic bone cells. *Environmental Health Perspectives*, 84(1), 99-106. https://doi.org/10.1289%2Fehp.908499

Tsien, R. Y. (1980). New calcium indicators and buffers with high selectivity against magnesium and protons: design, synthesis, and properties of prototype structures. *Biochemistry*, *19*(11), 2396-2404. https://doi.org/10.1021/bi00552a018

Willcott, M. R. (2009) MestRe Nova. *The Journal of American Chemical Society*, 131, 13180–13180. https://doi.org/10.1021/ja906709t

Zhou, X., Belavek, K. J., & Miller, E. W. (2021). Origins of $Ca^{2+}$ Imaging with Fluorescent Indicators. *Biochemistry*, *60*(46), 3547-3554. https://doi.org/10.1021/acs.biochem.1c00350.